Cycle life and statistical predictive reliability model for all-solid-state thin film microbatteries

Nathanaël Grillon, Emilien Bouyssou, Sebastien Jacques, Gaël Gautier

Cycle Life and Statistical Predictive Reliability Model for All-Solid-State Thin Film Microbatteries

Nathanaël Grillon[a,b*], Émilien Bouyssou[a], Sébastien Jacques[b], Gaël Gautier[b]

[a] STMicroelectronics Tours, 10, rue Thalès de Milet, CS97155, 37071 Tours Cedex

[b] Université de Tours, CNRS, INSA-CVL, GREMAN UMR 7347, 16 rue Pierre et Marie Curie 37100 Tours, France

*Corresponding author. Tel.: +33 2 47 42 40 00; fax: +33 2 47 42 49 70

E-mail address: nathanael.grillon@st.com

Abstract: This paper focuses on the development of a predictive cycle life model of all-solid-state thin film Cu / Li / LiPON / $LiCoO_2$ microbatteries based on experimental accelerated aging tests. More than 120 samples were tested in 8 different conditions including several electrochemical cycling modes and different temperature levels. Hence, an original reliability model, based on an exponential function especially designed to describe the degradation mechanism occurring at the positive electrode, is proposed to describe the observed capacity loss evolution of microbatteries. An extended mathematical model, which includes a large set of accelerated factors, physicochemical considerations and statistical parameters is then built around such an exponential function. This model thus enables to simulate a wide variety of battery aging profiles from input parameters such as temperature, depth of charge (*DoC*), discharge rate, failure rate and capacity fade. We believe that the development of such a reliability model is of most importance not only from an industrial point of view, since it enables to determine precisely the expected behavior of microbatteries in various mission profile conditions, but it represents also a key tool that enables to further understand the observed degradation mechanisms, and to identify any technological optimization opportunities.

Keywords: Microbattery; Cycle life; Aging modeling; Reliability

1. Introduction

The recent and rapid progress in micro/nano-electromechanical system technologies have largely reduced the size, current density and power requirement of electronic devices to extremely low levels [1]. Today, conventional lithium ion batteries are extensively used due to their large capacities, but they still present serious safety issues due to the presence of liquid electrolyte and separators. Besides, lithium-polymer battery technologies, despite their interesting mechanical and compact design characteristics, still suffer from failure mechanisms issues related to dendritic growth [2-4], which is likely to induce some risks of explosion [5]. Accordingly, these safety and reliability limitations have led to the emergence and the development of all-solid-state thin film systems [6,7]. In 1990s, Bates *et al*. reported and patented rechargeable all-solid-state lithium batteries in Oak Ridge National Laboratory, resulting in the recent development of new thin film energy storage systems [8]. With the rise of new efficient positive electrode materials ($LiCoO_2$, $LiMn_2O_4$ [9]) and electrolyte components [10] for all-solid-state implementation, thin film microbatteries aroused interest for manufacturers of embedded electronics and Internet Of Things (*I.O.T.*) systems. In Figure 1 we propose a classification of lithium-ion secondary battery technologies as a function of the nature of their electrolyte.

Hence, all-solid-state thin-film lithium microbatteries, characterized by a total thickness lower than 100 µm, fulfill the requirements of a wide range of new markets and applications, such as smart cards, battery-assisted RFID tags, wireless sensor networks, and multiple advanced healthcare applications [11,12]. Innovative due to the absence of liquid electrolyte, these systems present many advantages over conventional lithium cells. Eco-friendly, it avoids any

chemical leakage and improves thermal stability. Moreover, the solid/solid interfaces are stable and less prone to morphological and chemical modifications, such as dendrite formation whenever metal lithium is used as negative electrode or solid/electrolyte interphase growth at the surface of the negative electrode.

Whatever their electrochemical and architectural properties, battery devices are promptly the topics of cycle life studies through more or less thorough reliability analyzes. The reliability of an element represents the probability that this element performs a given function correctly under defined stresses for a certain time interval. Hence, the demonstration and the control of reliability performances have clearly become a major industrial challenge for new technologies qualification. However, the qualification phase of any new technology is not expected to exceed a few months, so it is merely impossible to evaluate in real conditions the components under development, since the lifetime of such component in operating conditions is requested to reach up to 10 years. That is the reason why it becomes necessary to perform accelerated aging tests to guarantee a certain level of reliability performances, through the development of a predictive reliability model.

The equations proposed in the literature to model the degradation of conventional liquid electrolyte batteries are mostly based on the description of the growth mechanisms of the *SEI* (*Solid Electrolyte Interface*) at the negative electrode [13-15]. In a few studies, the growth of an oxide film at the positive electrode is also considered [16]. Whether the models assign to the irreversible loss of capacity by the growth [17,18] and/or the dissolution of *SEI* [19], they all represent the aging as a function of the square root of either the time, $f(t) = t^{1/2}$, or the number of cycles, $f(n) = n^{1/2}$. Such a model is assumed to express the loss of capacity by the unidimensional limitation of diffusion phenomena within the *SEI* during its growth, with a

quite accurate adjustment of experimental aging data, as reported by Ozawa [20]. Such degradation mechanism turns out to be thermally activated. Hence, the aging of conventional batteries, defined by Equation 1, associates a square root function to describe the time evolution of the capacity fade, with an Arrhenius law to take into account the temperature dependency [21].

$$\Delta Q/Q_0 = A.t^{1/2} = B.exp\left(\frac{-Ea}{kT}\right).t^{1/2} \qquad 1$$

$\Delta Q/Q_0$ represents the relative capacity fade, B is a pre-exponential factor, k is the Boltzmann constant, T is the temperature and Ea is the activation energy of the mechanism.

Although this model structure is accepted and commonly used by the scientific community, it remains limited to temperature effect description, and does not enable to take into account complex mission profiles. Moreover, this model appears to be incomplete for reliability considerations, since it does not provide any statistical indication of expected failure rate, which is clearly becoming a mandatory information to figure out. It is indeed naturally essential for a manufacturer to be able to provide a given lifetime associated with a failure rate level, reflecting the exact likelihood that the product will meet the expected performances.

Because of their recent development, all-solid-state microbattery technologies have been the topic of only few reliability studies, which mostly deal with operating characteristics [8,22,23], failure mechanisms [24,25], and capacity loss after a reduced number of cycles [26]. The objective of this study is therefore to propose a complete reliability model that predicts the cycle life of all-solid-state thin film microbatteries in application conditions,

integrating a large number of operational parameters as input data, including the expected failure rate as a statistical feature.

2. Experimental test procedure

2.1.Cell structure and cell testing procedure

This experimental study focuses on the reliability performances of *EnFilm EFL1K0A39* microbatteries manufactured by STMicroelectronics Tours (France). This device is characterized by 1×1 inch footprint and a nominal capacity of 1.0 mA.h between 4.2 V and 3.0 V. As can be seen from Figure 2, the positive electrode material is made of lithium cobalt oxide ($LiCoO_2$). The solid electrolyte is composed of lithium phosphorus oxynitride (LiPON) [27]. Both the two thin films are deposited using radio frequency magnetron sputtering techniques and the total thickness of the active layers does not exceed 20 μm.

In order to evaluate their reliability behavior, the microbatteries were submitted to series of potentiodynamic charges and galvanostatic discharges. The maximum capacity is delivered over a voltage range between 4.2 V and 3.0 V. The thermal conditioning was carried out in an environmental test chamber (ESPEC North America, Hudsonville, USA) operating within a temperature range between - 40°C and +80°C with an accuracy of ±1°C. The electrochemical cycling tests were performed by the means of MPG-2 multi potentiostat/galvanostat systems (Biologic, Claix, France). Five control measurements, including potentiostatic charges and galvanostatic discharges, from *n=0* cycle (pristine state) up to *n=500* cycles were performed for each test conditions, in order to quantify the aging of

the microbatteries through the capacity fade analysis. These electrochemical readout experiments were carried out at 30°C on a VMP versatil multi potentiostat.

2.2.Cycle life measurement

Accelerated cycle life testing consisted in exposing battery cells to the conditions given in the test matrix described in Table 1, which represents 8 different test conditions. These conditions include three temperatures levels (45°C, 60°C, and 80°C), four depth of charge (100%, 75%, 50% and 25%) and three discharge rates (2C, C, C/10). Up to 16 batteries were tested in each condition. Hence, a total amount of 128 batteries were necessary to complete the experimental procedure proposed in this reliability study.

To evaluate the aging of the batteries according to the state of charge, the depth of charge (*DoC*) was introduced as a new operating parameter. Indeed, reliability studies of battery systems conventionally evaluate aging as a function of the depth of discharge (*DoD*). In this case, the batteries are always charged to the maximum working voltage and discharged to intermediate voltages. In our study, the microbatteries were systematically discharged until 3.0 V and charged at different intermediate voltage levels between 3.0 V and 4.2 V, corresponding to 0% *DoC* and 100% *DoC* respectively. Experimentally, the operating voltages corresponding to each considered depth of charge were preliminary determined from the nominal delivered capacity between 4.2 V and 3.0 V for each battery sample.

3. Results and modeling

3.1.Experimental aging data

The mean relative capacity loss obtained as a function of temperature is represented in Figure 3.

As expected, the capacity fade is observed to increase as the temperature increases, which is consistent with the temperature dependency of aging reported elsewhere [17,18,21]. Besides, the evolution of capacity fade as a function of the depth of charge level is exhibited in Figure 4. The aging trend is clearly accelerated as the depth of charge level increases, which can also be considered as an expected result based on the known behavior of conventional batteries.

On the contrary, the results of aging as a function of the discharge rate appears to be less intuitive. As can be seen in Figure 5, the cycle life is observed to be enhanced when stronger discharge currents are applied. Such results are effectively contrary to the effects described in the literature for most conventional batteries [28,29], for which the aging generally turns out to be accelerated at higher current regime. We believe that the decrease of cycle life at lower current regime for our microbattery technology may be associated to the longer time spent in such a case in higher charge state, corresponding to lower lithiation states for the $LiCoO_2$ positive electrode. Indeed, the storage at low lithiation states is known to accelerate the capacity fade mechanisms, as already reported by several research groups [30-32]. Such an effect is attributed to the degradation of the electrochemical properties of the $LiCoO_2$ positive electrode material by chemical dissolution or modification of its active structure. Therefore, for high discharge rate conditions, less time is spent at lowest lithiation states of $LiCoO_2$ material, which would tend to limit the degradation mechanisms, compared to lower current regimes.

3.2.Modeling of aging data

For all-solid-state microbattery technologies, the main aging contributor appears to be the positive electrode. Indeed, the major source of capacity loss for a Li / LiPON / $LiCoO_2$ microbattery system was demonstrated to be the degradation of the physico-chemical properties of the $LiCoO_2$ material [24]. Fine analyzes have also shown that the aging is caused by the growth of a disordered interphase layer between the LiPON electrolyte and the positive electrode due to the decomposition of the $LiCoO_2$ into disordered rocksalt like cobalt oxide, Li_2O and Li_2O_2. During cycling, the disordered layer consumes the electrochemically active cathode layer, reducing the overall capacity [33]. These results make it possible to consider the aging of all-solid-state microbatteries as the consequence of a continuous accumulation of intrinsic defects within the positive electrode during the electrochemical cycling. In order to model the observed experimental data, we propose to introduce a general exponential mathematical law that can describe a wide range of physical behaviors. The considered mathematical structure describes the loss of initial capacity ($\Delta Q/Q_0$) as a function of the number of cycles (n), as shown in Equation 2:

$$\Delta Q/Q_0 = 1 - exp^{-\left(\frac{n}{\tau}\right)^{\alpha}} \qquad 2$$

Such a relation is based on the general description of a transient evolution between two equilibrium states, characterized by a time constant τ reflecting the speed of the evolution. Hence, in our case, the τ parameter is defined as the number of cycles leading to a capacity loss of 63.2%, and can be considered as a characteristic of the aging kinetics. Indeed, for a

cycle number $n = \tau$, the relative capacity loss is equal to $1\text{-}exp^{-1}$, namely 63.2%. The α parameter can be perceived as a shape parameter, which reflects the more or less steep character of the degradation. The fitting results of the experimental data obtained by Equation 2 are exhibited in Figure 6. The shape parameter α turns out to remain constant for all the experimental trends, with a mean value of 0.55 ± 0.02, whereas the evolution of the τ parameter depends on the various studied conditions as shown in Table 2.

The mean relative deviation between the modeling results and the experimental data is below 10%, which can be considered as quite satisfying, and which tends to validate the relevance of the choice of the mathematical model proposed in Equation 2. Hence, such an empirical model structure turns out to be a good alternative to the square root model often used to describe the aging of conventional liquid electrolyte batteries, which would be meaningless in the case of all-solid-state microbatteries, due to the absence of Solid Electrolyte Interface in the negative electrode.

3.3.Model parameters extraction

From the Equation 2, the number of cycles (n) can be expressed as a function of capacity loss ($\Delta Q/Q_0$), τ parameter and α parameter. As shown in Equation 3, it is possible to express the cycle life as:

$$n = \tau . \left(-ln(1 - \Delta Q/Q_0)\right)^{1/\alpha} \qquad 3$$

To integrate a wide range of mission profiles, the cycle life calculation must express the aging dependence of the batteries as a function of temperature, depth of charge and discharge

current rate. Hence, an expression of the τ parameter has to be developed to account for such dependencies. As can be seen in Figure 7-a, the temperature dependence of aging can be described by an Arrhenius law (Equation 4), with an activation energy of 0.86 ± 0.05 eV.

$$\tau = C . exp(Ea/kT) \quad (4)$$

In the same way, an exponential evolution of the τ parameter is obtained regarding the *DoC* (Figure 7-b) and the discharge rate (Figure 7-c) effects, with δ and ι defined as the acceleration parameters, reflecting respectively the aging dependence of the microbatteries as a function of the depth of charge and the discharge rate:

$$\tau = C' . exp(-\delta . DOC - \iota . I) \quad (5)$$

Hence, by developing the Equation 3 formula, the extrapolation of the lifetime can be now on calculated as:

$$n = A.\left(-ln(1 - \Delta Q/Q_0)\right)^{1/\alpha} . exp\left(Ea/_{k.T} - \delta . DoC - \iota I\right) \quad (6)$$

Where A = 5.664×10^{-10} cycles as a pre-exponential empirical constant, α = 0.55 the capacity fade shape parameter, Ea = 0.86 eV as the activation energy of the degradation mechanisms, k = 1.381×10^{-23} J.K^{-1} the Boltzmann constant, δ = 4.11 as the acceleration parameter related to the depth of charge and ι = 0.68 mA^{-1} as the acceleration parameter related to the discharge rate.

3.4.Statistical study

To complete the reliability model development, a failure rate function (*F*) is introduced as an input parameter. The failure rate can be defined as the probability for the battery to exceed a critical capacity loss. Such failure criterion is defined in our study by an irreversible capacity loss of 20% compared to the initial capacity of the system. Hence, a statistical analysis of the cycles to failure n_f observed in given operational conditions can be carried out, by the means of the Weibull probability law.

The Weibull cumulative distribution function, is commonly used in reliability analysis, as it can express a wide variety of failure modes [34-36]. As can be seen in Equation 7, the failure distribution in the Weibull law is defined by two parameters: the shape parameter β and the scale parameter η. The scale parameter η is defined as the number of cycles leading to the failure of 63.2% of batteries within a given battery population. This scale parameter depends directly on the test conditions, whereas the shape parameter β should remain constant on the experimental conditions range, since it represents a characteristic signature of the involved failure mechanism.

$$F(n_f) = 1 - exp^{-\left(\frac{n_f}{\eta}\right)^{\beta}} \qquad 7$$

Note that the correspondence of the mathematical structures of equations 2 and 7 has to be considered as a coincidence. The first one describes the gradual capacity loss $\Delta Q/Q_0$ evolution during cycling, whereas the second one describes the evolution of the failure rate *F*, namely the proportion of failed batteries within an initial population submitted to cycling

tests, considering the failure criterion of 20% capacity loss. From Equation 7, the cycle to failure can be expressed as a function of the failure rate (*F*) as exhibited in Equation 8:

$$n_f = \eta\left(-ln(1-F)\right)^{1/\beta} \quad (8)$$

By performing a linearization of Equation 8, it is possible to graphically represent the distribution of cycles to failure, considering the β parameter as the slope of the distribution represented in a log scale, as shown in Equation 9:

$$ln\left(ln\left(\frac{1}{1-F}\right)\right) = \beta.ln(n_f) - \beta.ln(\eta) \quad (9)$$

The cycles to failure are extracted from each sample of each accelerated aging test condition. The values of the shape parameter β determined for each experimental condition are gathered in Table 3.

Graphically, an example of probability plot obtained for the cycles to failure considering three different experimental conditions is shown in Figure 8.

The mean value of the shape parameter β obtained for the set of temperature conditions is 3.5 ± 1.5. For the distribution of the cycles to failure according to the different considered *DoCs*, the average value of β is 3.0 ± 1.1. Finally, for the different considered discharge rates, the value of the β parameter is 3.5 ± 1.7. These results tend to prove a noticeable homogeneity of the values of the β parameter. This homogeneity reflects the expression of a same failure

mechanism affecting the microbatteries under the whole electrochemical cycling conditions deployed in our study.

This statistical analysis thus demonstrates that the aging of the all-solid-state microbatteries results from a unique physicochemical failure mechanism, thermally activated, dependent not only on the state of charge, but also on the applied current regime.

3.5.Cycle life and statistical prediction tool

Considering Equation 8, the general mathematical structure of the predictive reliability model described by Equation 6 can now be completed to express the cycle life as a function of the capacity fade, the temperature, the depth of charge, the discharge regime and the failure rate as shown below:

$$n_f = A.\left(-ln(1-\Delta Q/Q_0)\right)^{1/\alpha}.exp\left(Ea/_{k.T} - \delta.DoC - \iota.I\right).\left(-ln(1-F)\right)^{1/\beta} \quad 10$$

With β = 3.3 the average statistical Weibull shape parameter, characteristic of the observed failure mechanism at the origin of the studied aging.

4. Discussion

The cycle life of microbatteries during electrochemical cycling is described for the first time as a function of different input parameters including environmental criteria and operating conditions. Unlike the classical square root model that describes the aging of conventional battery technologies, the global model developed in the present study makes it possible to

propose a statistical dimension of the modeling result, by taking into account the expected failure rate in any application mission profile.

To illustrate the interest of our predictive tool, an example of implementation of the model for the cycle life extrapolation of microbatteries in realistic applications can be proposed. Considering a typical operational use at a temperature of 25°C, over the working range of 75% *DoC*, at 1C current regime, a capacity loss of 20% can be predicted after 4,470 cycles, for 0.1% of the considered samples. Our model is thus able to provide an extrapolated cycle life response to a specific mission profile, but it also offer the possibility to determine any better alternatives of application conditions. For instance, the model enables to forecast that a limitation of temperature below 21°C will enhanced, in the given example, the cycle life up to 7,000 cycles, and the same result would be achieved by reducing the *DoC* down to 64%.

5. Conclusion

In this paper, the intrinsic reliability performances of all-solid-state microbatteries were evaluated. The analysis of experimental irreversible capacity loss data has revealed that the capacity fade of batteries was accelerated by various environmental and operational factors, such as temperature, depth of charge, and discharge rate. Therefore, a reliability model based on an exponential function has been proposed to fit the aging data. This exponential law, assumed to describe a process of continuous loss of active material within the $LiCoO_2$ positive electrode, has been observed to be very suitable for the case of all-solid state battery system. Indeed, this exponential law makes it possible to overcome the insufficient justification of the use of a function defined by the square root of time, or by the square root of the number of cycles, generally deployed for modeling the diffusion phenomena within the

specific *SEI* layer of conventional battery technologies. Moreover, the use of this exponential law has made it possible to extract acceleration factors reflecting the dependence of the aging of microbatteries with the temperature, with the lithiation state of $LiCoO_2$ material and with the discharge rate. In addition, the statistical analysis of the accelerated aging data allowed us to identify the signature of a single failure mechanism at the origin of the observed performances. Characterized by a Weibull shape parameter β of 3.3, this degradation mechanism is proved to be independent of the operating mode applied to the electrochemical cells. Finally, this study led to the development of a predictive cycle life calculation tool, integrating the possibility for the user to consider different operating conditions, as well as a statistical dimension through the failure rate determination.

Acknowledgments

This work was performed in the frame of TOURS 2015, project supported by the French "Programme de l'économie numérique des investissements d'avenir".

References

[1] N. J. Dudney, B. J. Neudecker, Curr. Opin. Solid ST. M 4 (1999) 479-482.

[2] J.-N. Chazalviel, Physical Review A, 42 (1990) 7355.

[3] C. Brissot, M. Rosso, J.-N. Chazalviel, P. Baudry, S. Lascaud, Electrochim. Acta 43 (1998) 1569-1574.

[4] M. Rosso, C. Brissot, A. Teyssot, M. Dollé, L. Sannier, J.-M. Tarascon, R. Bouchet, S. Lascaud, Electrochim. Acta 51 (2006) 5334-5340.

[5] A. Gibbs, *Lithium Polymer Batteries*, A Gibbs Guide ebook (2013).

[6] J. B. Bates, N. J. Dudney, B. Neudecker, A. Ueda, C. D. Evans, Solid State Ionics 135 (2000) 33-45.

[7] J. B. Bates, G. R. Gruzalski, N. J. Dudney, C. F. Luck, X. H. Yu, Solid State Ionics 70 (1994) 619-628.

[8] J. B. Bates, N. Dudney, G. Gruzalski, C. F. Luck, U. S. Patent 5338625 (1992).

[9] K. Ozawa, Lithium Ion Rechargeable Batteries: Materials, Technology, and New Applications, *Wiley-VCH,* (2012) p. 257-259.

[10] I. Seo, and S. W. Martin, New Developments in Solid Electrolytes for Thin Film Lithium Batteries, *Ilias Belharouak* (2012).

[11] N. J. Dudney, The Electrochem. Society Interface 17 (2008) 44-48.

[12] A. T. Kutbee et al., Flexible Electronics 1 (2017) 7.

[13] D. Aurbach, J. of Power Sources 89 (2000) 206-218.

[14] M. Safari, M. Morcrette, A. Teyssot, C. Delacourt, J. Electrochem. Society 156 (2009) A145-A153.

[15] M. Broussely, S. Herreyre, P. Biensan, P. Kasztejna, K. Nechev, R. J. Staniewicz, J. of Power Sources 97-99 (2001) 13-21.

[16] P. Ramadass, B. Haran, R. White, B. N. Popov, J. of Power Sources 112 (2002) 606-613.

[17] R. B. Wright et al., J. of Power Sources 110 (2002) 445-470.

[18] R. Spotnitz, J. of Power Sources 113 (2003) 72-80.

[19] R. Spotnitz, in: M. Anderman (Ed.), Proceedings of the 2nd Adv. Auto. Battery Conference (AABC-02) (2002).

[20] Y. Ozawa, R. Yazami, B. Fultz, J. of Power Sources 119 (2003) 918-923.

[21] I. Bloom et al., J. of Power Sources 101 (2001) 238-247.

[22] J. L. Souquet, M. Duclot, Solid State Ionics 148 (2002) 375-379.

[23] S. D. Fabre, D. Guy-Bouyssou, P. Bouillon, F. Le Cras, C. Delacourt, J. Electrochem. Society 159(2) (2012) A104-A115.

[24] N. Grillon, E. Bouyssou, S. Jacques, G. Gautier, J. Electrochem. Society 162(14) (2015) A2847-A2853.

[25] Z. Wang et al., J. of Power Sources 324 (2016) 342-348.

[26] G. Nagasubramanian, D. Doughty, J. of Power Sources 136 (2004) 395-400.

[27] X. Yu, J. B. Bates, G. Jellison, F. Hart, J. Electrochem. Society 144 (1997) 524-532.

[28] S.S. Choi, H.S. Lim, J. of Power Sources 111 (2002) 130-136.

[29] G. Ning et al., J. of Power Sources 117 (2003) 160-169.

[30] J. Li, J. Zhang, X. Zhang, C. Yang, N. Xu, B. Xia, Electrochim. Acta 55 (2010) 927-934.

[31] Y. Ozawa, R. Yazami, B. Fultz, Electrochem. and Solid-State Letters, 8 (2005) A38-A41.

[32] S. Choi, A. Manthiram, J. Electrochem. Society 149 (2002) A162-A166.

[33] Z. Wang et al., J. of Power Sources 324 (2016) 342-348.

[34] R. B. Abernethy, *The New Weibull Handbook* (1996).

[35] C. M. Harman, J. of Power Sources 37 (1992) 363-368.

[36] S.-W. Eom, M.-K. Kim, I.-J. Kim, S.-I. Moon, Y.-K. Sun, H.-S. Kim, J. of Power Sources 174 (2007) 954-958.

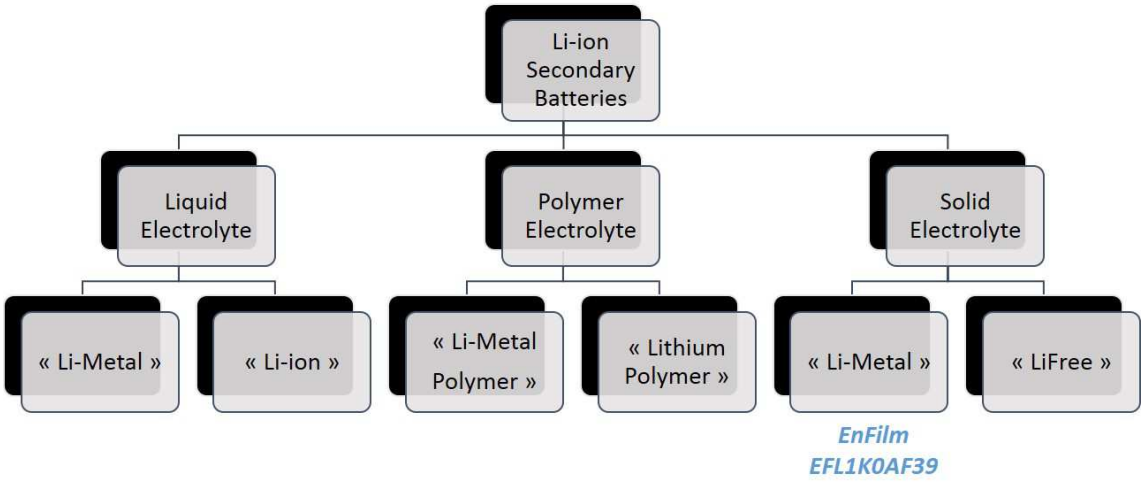

Fig. 1: Classification model of lithium-ion secondary battery technologies. “Li-metal” refers to the integration of a negative electrode composed of metallic lithium. For other types of technologies, lithium is only in ionic form.

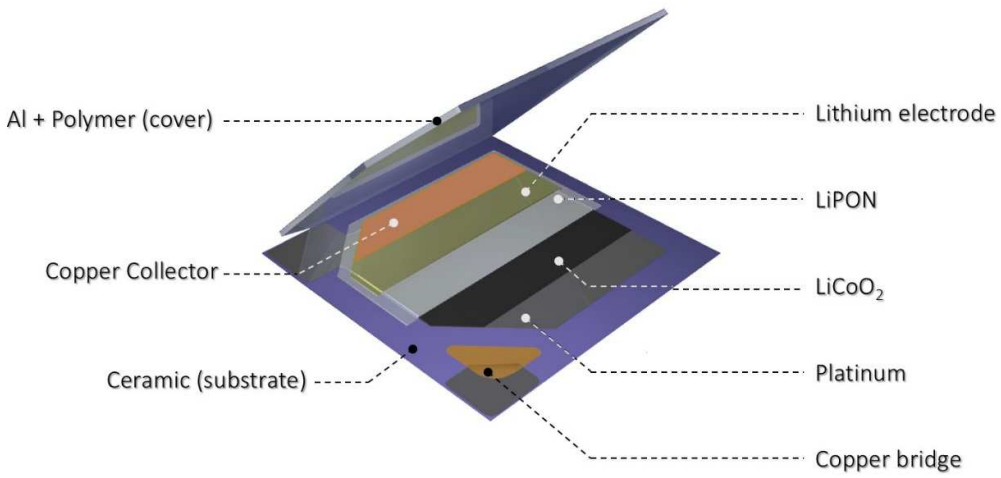

Fig. 2: Schematic representation of the EnFilm EFL1K0AF39 microbatteries.

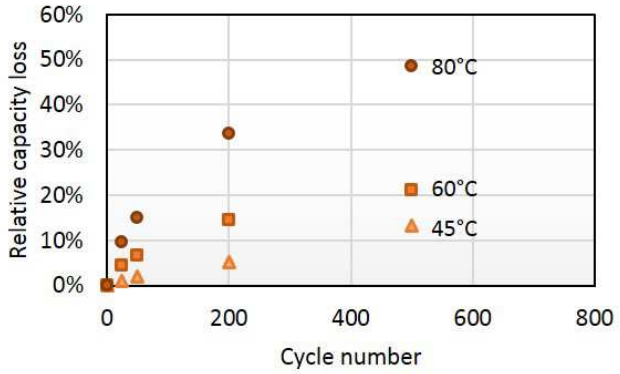

Fig. 3: Mean relative capacity loss as a function of temperature, for cycling tests performed at 100% *DoC*, 1C for 3 different temperatures (45, 60 and 80°C). All measurement readouts are carried out at 30°C.

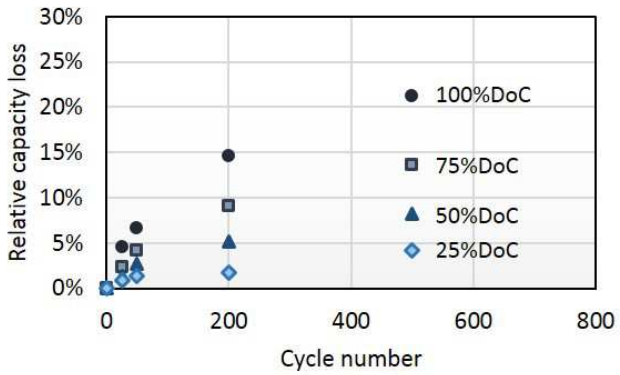

Fig. 4: Mean relative capacity loss as a function of the *DoC*, for cycling tests performed at 60°C, 1C for 4 different *DoC* (25, 50, 75 and 100%). All measurement readouts are carried out at 30°C.

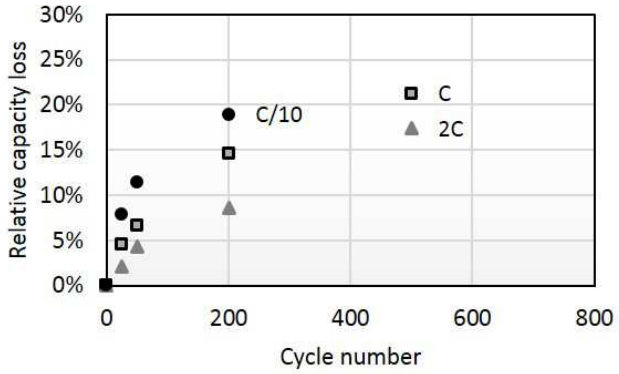

Fig. 5: Mean relative capacity loss as a function of the discharge rate at T=60°C, 100% *DoC* for 3 different discharge currents (C/10, C and 2C). All measurement readouts are carried out at 30°C.

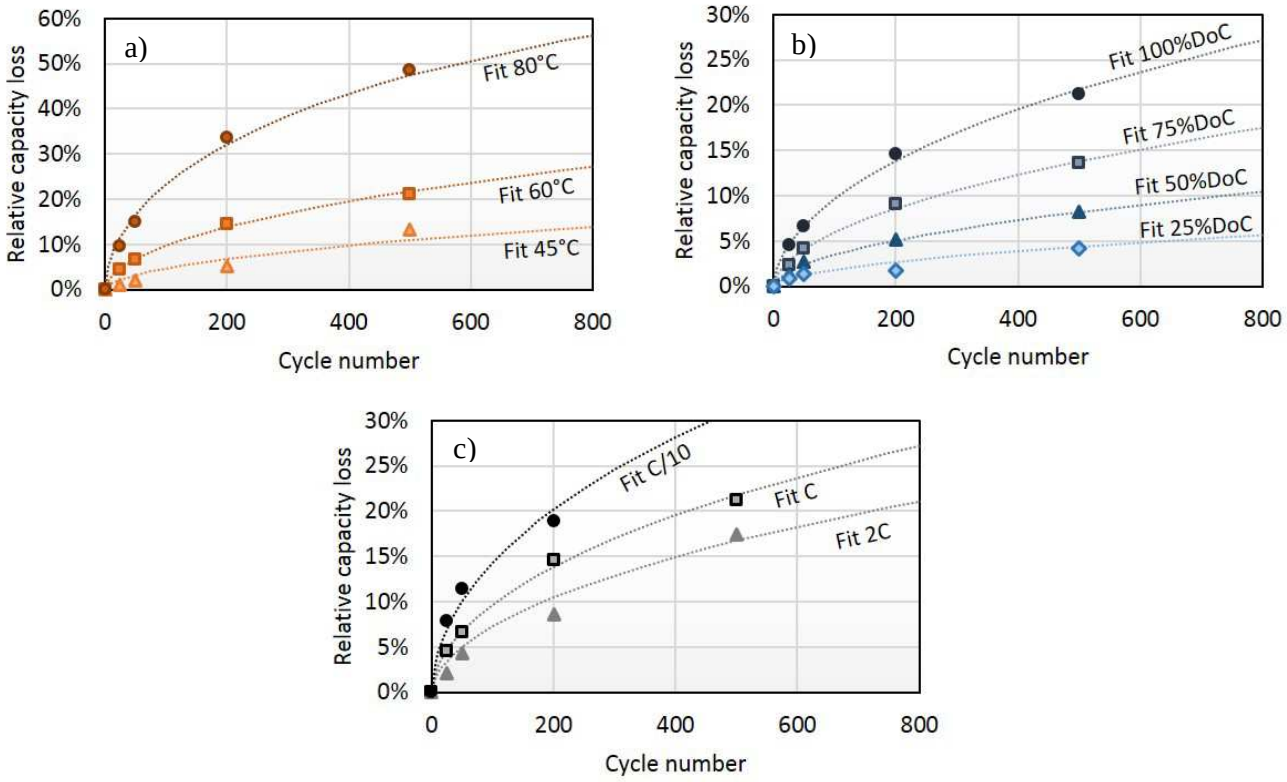

Fig. 6: Fitting results of the experimental data for a) accelerated aging test as a function of the temperature b) accelerated aging test as a function of the depth of charge c) accelerated aging test as a function of the discharge rate.

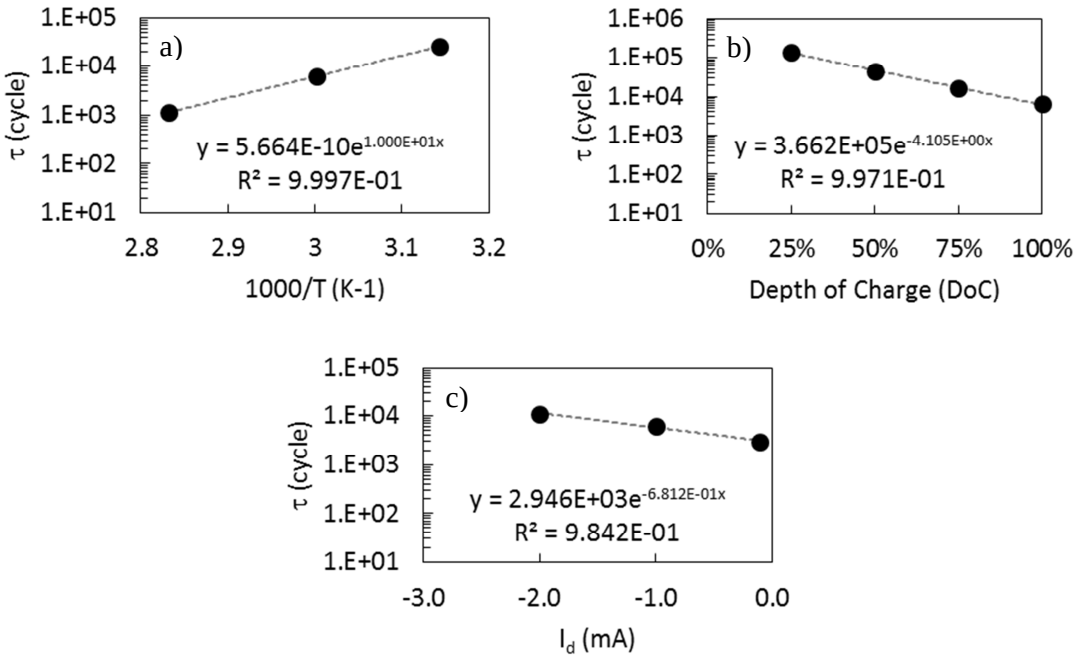

Fig. 7: Expression of the scale parameter (τ) as a function of a) temperature by means of an Arrhenius law b) considered depths of charge c) considered discharge currents. The scale parameter τ represents the number of cycles for which a level of 63.2% of capacity loss is reached.

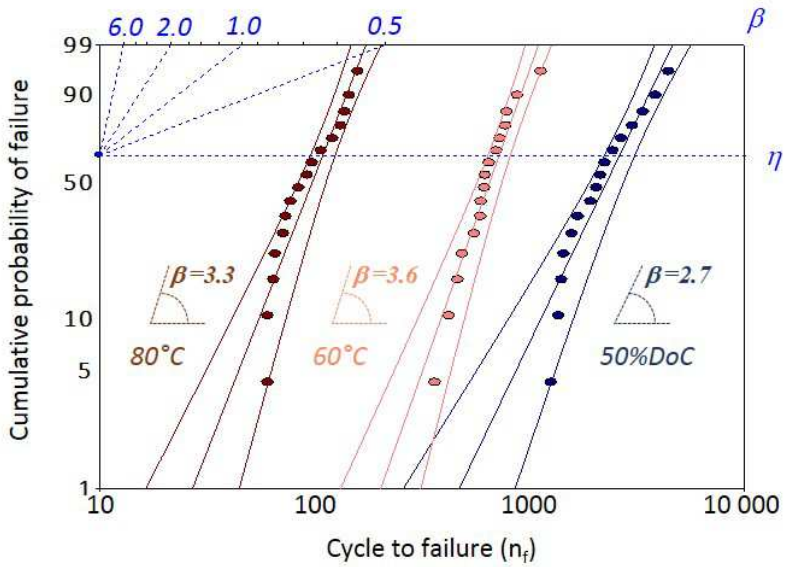

Fig. 8: Cumulative distributions plot of cycles to failure n_f for conditions 80°C/*100% DoC*/C, 60°C/*100% DoC*/C and 60°C/*50% DoC*/C. The curved lines represent the corresponding two-sided approximate 95% confidence limits for the function. The cycle to failure is determined considering a failure criterion of 20% irreversible capacity loss.

Tables

Table 1

Experimental matrix of test conditions.

DoC (C rate)	*Temperature*		
	45°C	60°C	80°C
100%	×	×	×
75%		×	
50%		×	
25%		×	
I_d (100%DoC)			
2.0 mA (2C)		×	
0.1 mA (C/10)		×	

Table 2

Extracted values of the scale parameter (τ) for each considered test conditions.

DoC (C rate)	*Temperature*		
	45°C	60°C	80°C
100%	25,200 cy	6,400 cy	1,120 cy
75%		16,000 cy	
50%		43,800 cy	
25%		140,000 cy	
I_d (100%DoC)			
2.0 mA (2C)		11,010 cy	
0.1 mA (C/10)		3,000 cy	

Table 3

Extracted values of the Weibull shape parameter (β) for each considered test conditions.

DoC (C rate)	*Temperature*		
	45°C	60°C	80°C
100%	3.7 ± 2.1	3.6 ± 1.3	3.3 ± 1.2
75%		3.3 ± 1.2	
50%		2.7 ± 0.9	
25%		2.5 ± 1.1	
I_d (100%DoC)			
2.0 mA (2C)		3.3 ± 1.8	
0.1 mA (C/10)		3.5 ± 1.9	